Passively *Q*-switched microchip laser at 1.5 μm

R. Häring, R. Paschotta, R. Fluck,* E. Gini, H. Melchior, and U. Keller

Institute of Quantum Electronics, Swiss Federal Institute of Technology (ETH), ETH Hönggerberg HPT, CH-8093 Zürich, Switzerland

Received February 23, 2001; revised manuscript received May 30, 2001

We demonstrate a compact laser source in the eye-safe wavelength regime ($\approx$1.5 μm) that produces peak powers up to 10.6 kW at pulse durations of 0.84 ns with a repetition rate exceeding 1 kHz. An Er:Yb:glass microchip laser was passively *Q*-switched with a semiconductor saturable absorber mirror (SESAM). We investigated SESAM damage under *Q*-switching conditions and developed an improved SESAM design that can withstand microjoule pulses. © 2001 Optical Society of America

OCIS codes: 140.3540, 140.3330, 140.3500, 140.3480, 230.4320, 140.3580.

1. INTRODUCTION

Applications involving free-space propagation of short laser pulses can take advantage of much higher peak and much higher average power when the wavelength regime near 1.5 μm is used. In this spectral range the light is strongly absorbed in the water-rich parts of the eye, and does not reach the sensitive retina. Applications for such sources include sensing of gases and contamination in air, distance measurements, and three-dimensional imaging. Different approaches for adequate laser sources have been reported in recent years. Peak powers of >100 kW and pulse durations of <200 ps have been reported with frequency conversion in an optical parametric generator.[1,2] Gain switching of a Cr^{4+}:YAG laser pumped with a *Q*-switched Nd:YAG microchip laser was demonstrated recently.[3] A more direct, simple, and efficient approach is passive *Q* switching of a 1.5-μm laser with an absorber crystal (e.g., Co^{2+}:$LaMgAl_{11}O_{19}$,[4,5] Er:$Ca_5(PO_4)_3F$,[6] U^{4+}:CaF_2,[7,8] U^{4+}:SrF_2,[9] Co^{2+}:ZnSe,[10] Cr^{2+}:ZnSe[11]) or with a semiconductor saturable absorber mirror (SESAM).[12] Laser emission at ~1.5 μm has been reported from several gain materials including Cr^{4+}:YAG (review on Cr^{4+}-doped garnets),[13] Yb^{3+}:Tm^{3+}:$YLiF_4$,[14] Er:Ti:$LiNbO_3$,[15] and, most commonly used for diode-pumped bulk lasers, Er:Yb:glass.[16]

SESAMs[17,18,19] have been extensively used for passive mode locking and *Q* switching of solid-state lasers. Using a SESAM as a passive *Q* switch has a variety of advantages over other approaches. The flexibility of SESAMs allows tailoring of the parameters needed for a specific application. Design guidelines[20] for *Q*-switched microchip lasers with SESAMs can be used to vary the operation parameters in large ranges and can be applied to lasers operating in different wavelength regimes, e.g., at $\approx$1 μm,[21,22] $\approx$1.3 μm,[23] and $\approx$1.5 μm.[12] SESAMs allow us to realize a significantly shorter cavity length (in comparison with doped bulk crystals used as saturable absorbers) and therefore can be used to generate shorter pulses. Indeed, the shortest *Q*-switched pulse from a solid-state laser, 37 ps, has been achieved with a Nd:YVO_4 microchip laser with a SESAM.[20] Lasers with low thresholds and high efficiencies can be designed with SESAMs because the losses can be kept well below 1%. For example, we measured a threshold of 38 mW for a device emitting 0.85-μJ pulses at 1.5 μm with a 7-ns duration.

In our previous work for eye-safe microchip lasers,[12] peak power and pulse energy were limited by damage to the absorber. In this paper we present a strategy to obtain higher powers by designing SESAMs with a higher damage threshold. After this introduction, in Section 2 we describe the setup of passively *Q*-switched microchip lasers. In Section 3 we summarize the functional principle of these devices. In Section 4 we discuss some general aspects of SESAMs, the detailed structure for a 1.5-μm *Q*-switching element, and then a method to avoid damage to the absorber. In Section 5 measurements of the damage threshold under *Q*-switched laser operation for InP/InGaAsP SESAMs are presented. Finally, in Section 6 we report the performance of an optimized device.

2. MICROCHIP LASER SETUP

The setup of a microchip laser and the diagnostics is shown in Fig. 1. The cavity of a microchip laser consists of two parallel flat mirrors.[24] To be able to investigate a large variety of different laser parameters, we used discrete components for the output coupler, the gain medium, and the SESAM. Platelets of Er:Yb:glass (QX/Er from Kigre, Inc.) with 5 mm $\times$ 5 mm cross section were polished to thickness values of 0.2, 0.3. 0.5, 0.8, and 1 mm, respectively. The Er doping concentrations are 2.75 wt. % of Er_2O_3 for the thinner glasses (0.2–0.5 mm) and 2.2 wt. % for the thicker ones. The Yb co-doping is at a level of 21 wt. % of Yb_2O_3 for both melts. The polished faces were antireflection (AR) coated for both the laser and the pump wavelength. These glass plates were positioned with two molybdenum knives of 100 μm thickness, which touched from each side to allow free access to both faces. The output coupler approached the front face

while the SESAM was used from the other side to close the cavity. Air gaps of a few micrometers were left between the three components to allow for fine adjustment of the cavity. Compared with similar setups using other gain media such as Nd:YVO_4 or Nd:YAG, we found that the alignment of the output coupler and SESAM is much more delicate for Er:Yb:glass lasers. The reason for this is the negative dn/dT of the phosphate glass, which has a destablizing effect on the cavity mode. This effect competes with the stabilizing effects of thermal bulging of the end faces and gain guiding.[25,26] Small wedge angles of the order of a milliradian between the output coupler and the SESAM lead to a significant increase of the threshold and can affect the pulse shape. (This might lead to multiple pulses but can also significantly reduce the pulse duration.[27])

The laser is pumped with a 100-μm strip-width laser diode (Nortel Networks, Zürich). The diode can produce up to 3 W of pump power at 975 nm. However, we could apply only up to $\approx$1 W of pump power because we observed cracking of the glass at higher powers. We pumped the laser through a dichroic beam splitter and the output coupler.

The diagnostics were set up to monitor all the important parameters simultaneously. With a vidicon-tube camera we monitored the laser mode area and the transverse mode quality. We define the mode area as $\pi w^2/2$ (w is the Gaussian mode radius) so that the peak intensity (on the symmetry axis) is simply the power divided by the mode area. The repetition rate was determined with a 500-MHz digital oscilloscope. To measure the pulse shape and the pulse width we used a 45-GHz photodetector and a 50-GHz sampling head. The optical spectrum was monitored with an optical-spectrum analyzer with a resolution of 0.1 nm, and the average output power was measured with a thermal powermeter.

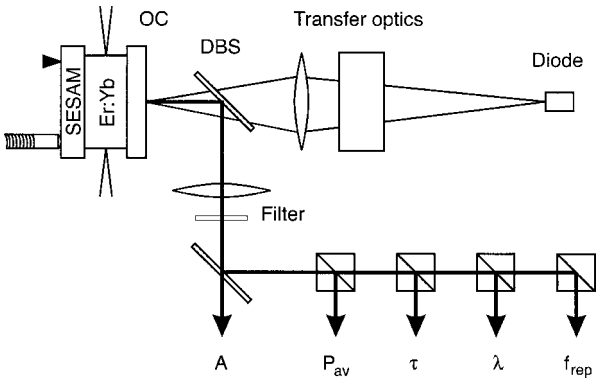

Fig. 1. Scheme of the laser and diagnostic setup. A polished and AR-coated Er:Yb:glass plate is held from the side by two knife edges. The output coupler (OC) and SESAM are aligned to be parallel within an angle of $<$0.1 mrad. We used up to 1 W pump power from a 100-μm strip width diode. The output is separated from the pump light with a dichroic beam splitter. (DBS). The output is divided with beam splitters to monitor several parameters simultaneously: A, laser mode area imaged with a vidicon tube camera; P_{av}, average power; τ, pulse duration measured with a 45-GHz detector and a 50-GHz sampling head; λ, optical spectrum; f_{rep}, repetition rate monitored with a digital oscilloscope.

3. OPERATION PARAMETERS OF *Q*-SWITCHED MICROCHIP LASERS

The dependence of the laser output on the design parameters has been described theoretically and confirmed experimentally by Spühler *et al.*[20] The model is based on a few assumptions that are usually well fulfilled by *Q*-switched microchip lasers:

1. Small gain and loss during 1 cavity round trip (a few percent) were assumed.
2. Spatial hole burning was neglected.
3. No transverse intensity variations within the area of the laser mode A_L were considered.
4. The total non-saturable losses (transmittance of the output coupler T_{OC} and parasitic losses l_{par}) are assumed to be larger than the modulation depth ΔR, which is favorable for both the slope efficiency and a symmetric pulse shape with short duration.

The modulation depth ΔR is defined as the amount of losses of the saturable absorber that can be bleached with high intensities. Here we summarize the most important results.

The pulse energy E_p can be written as

$$E_p = 2A_L F_L \Delta R \frac{T_{OC}}{T_{OC} + l_{par}}. \tag{1}$$

$$F_L = \frac{h\nu_L}{2\sigma_L + 2\sigma_L^{abs}}$$

is the saturation fluence of the gain material with ν_L the laser frequency and σ_L and σ_L^{abs} the cross section for stimulated emission and reabsorption at the laser wavelength, respectively. The fraction $T_{OC}/(T_{OC} + l_{par})$ accounts for the output coupling efficiency. To obtain a high pulse energy, one can enlarge the mode area, but a good beam quality cannot be obtained for modes that are too large. Choosing a gain material with a small gain cross section leads to a high saturation fluence and thus to a high pulse energy. Finally, the modulation depth of the SESAM can be increased, as is discussed in Section 4.

The pulse duration is given by[28]

$$\tau_p = \frac{7nL}{c\Delta R}, \tag{2}$$

where n is the index of refraction of the gain material, L is the cavity length, and c the speed of light. The cavity round trip time is $2nL/c$. A reduction of the pulse duration can be achieved by shortening of the cavity or by using a SESAM with larger modulation depth. Both measures, however, are limited by the requirement that sufficient gain must be generated to overcome the laser threshold.

The repetition rate is calculated as the average power divided by the pulse energy. As the pulse parameters are only weakly dependent on the pump power as long as the mode area is not significantly changed, an increase of pump power simply increases the repetition rate.

Er:glass has a high saturation fluence, and we can already achieve microjoule pulses with a modulation depth below 1%. These pulse energies can lead to SESAM

damage. To some extent, damage can be avoided by using improved SESAM designs as discussed in Section 4.

4. SEMICONDUCTOR SATURABLE ABSORBER MIRROR (SESAM)

A. Parameters of a SESAM

Figure 2 shows the reflectivity of a SESAM as a function of the incident pulse fluence. The modulation depth ΔR is defined as the maximum reflectivity change between low and high intensity. The remaining losses at high intensity we call nonsaturable losses, and the fluence needed to switch 1/e of the saturable losses is the saturation fluence F_{sat}. The dynamic response of the absorber plays a minor role for Q switching as long as the recovery time τ_{A} of the absorber is larger than the pulse duration τ_{p} and smaller than the pulse-to-pulse duration $1/f_{\mathrm{rep}}$. Having a recovery time shorter than the pulse duration reduces the efficiency of the laser but does not help to decrease the pulse duration. Therefore we typically use SESAMs with recovery times of several nanoseconds for Q-switched microchip lasers.

B. Top Reflector

The SESAM design best suited for Q switching with high pulse energies is the high-finesse antiresonant Fabry–Perot saturable absorber.[17,18] Here the semiconductor absorber is embedded in an antiresonant cavity between a semiconductor bottom Bragg mirror of high reflectivity and a sputtered dielectric top reflector with a transmittance T_{t} (Fig. 3).

An advantage of using a combined structure with semiconductor and dielectric materials is the possibility of characterizing the semiconductor structure before the top reflector is produced. Usually we cleave several samples of the same growth run and apply different dielectric coatings as a top reflector, where at least one sample has an AR coating for a high modulation depth that facilitates precise characterization. We call the modulation depth

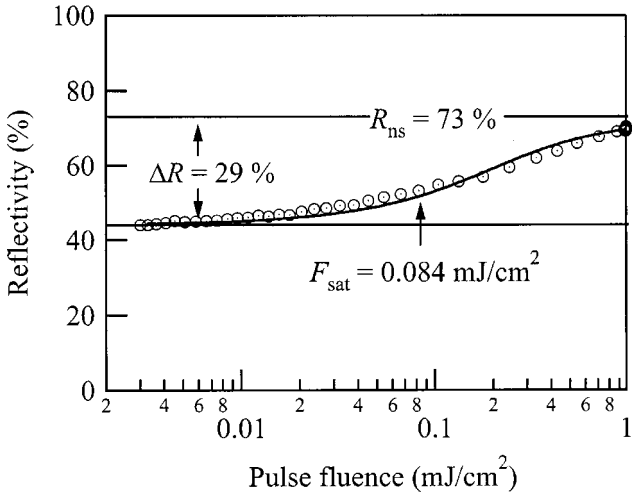

Fig. 2. Reflectivity of a SESAM as a function of the incident pulse fluence. The data were measured with 100-fs pulses from an optical parametric oscillator system. The SESAM is an AR-coated reference sample from the same growth run as SESAMs 8 and 9 in Table 1.

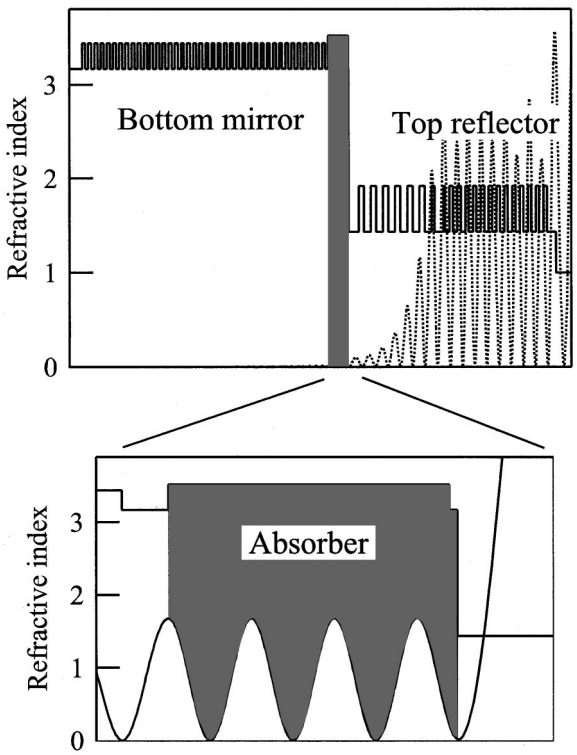

Fig. 3. Refractive-index profile and standing-wave pattern of SESAM 8 in Table 1. In the upper plot the bottom mirror and top reflector are well visible. The lower graph is a close up of the absorber region. The thickness of the absorber is adjusted so that the two mirrors are in antiresonance. The last semiconductor layer is a 21-nm thick InP cap layer to prevent surface recombination of the carriers.

of the AR-coated sample ΔR_{AR} and the nonsaturable losses $l_{\mathrm{ns,AR}}$ (or we specify the reflectivity in the saturated state $R_{\mathrm{ns,AR}} = 1 - l_{\mathrm{ns,AR}}$).

With the transmittance of the top reflector T_t we can adjust the intensity allowed to enter the absorber. Decreasing the transmittance T_{t} reduces the intensity on the absorber, and thus increases the damage fluence and reduces the nonsaturable losses, but also decreases the modulation depth and increases the saturation fluence. The fluence on the absorber F_{abs} can be calculated as[29]

$$F_{\mathrm{abs}} = \xi F_{\mathrm{AR}}, \tag{3}$$

where F_{AR} is the fluence in the AR-coated reference sample. For low fluences and in antiresonance the ξ factor can be written as

$$\xi_{\mathrm{low}} = \frac{T_t}{\{1 + [(1 - T_{\mathrm{t}})(R_{\mathrm{ns,AR}} - \Delta R_{\mathrm{AR}})]^{1/2}\}^2}. \tag{4}$$

In saturated condition ξ is

$$\xi_{\mathrm{high}} = \frac{T_t}{\{1 + [(1 - T_{\mathrm{t}})R_{\mathrm{ns,AR}}]^{1/2}\}^2}. \tag{5}$$

For small nonsaturable losses $l_{\mathrm{ns,AR}} \ll 1$ ($R_{\mathrm{ns,AR}} \approx 1$) the modulation depth is scaling with the same factor as the fluence for low intensities:

$$\Delta R \approx \xi_{\mathrm{low}} \Delta R_{\mathrm{AR}}, \tag{6}$$

where ΔR is the modulation depth of the sample with the top reflector.

C. SESAMs for 1.5-μm *Q*-Switching Experiments

The Bragg mirror and the absorber were grown with metal-organic chemical vapor deposition on an InP substrate. The materials used for the mirror as well as for the absorber were lattice matched to InP. For the bottom mirror, we used 40 pairs of InP/$In_{0.65}Ga_{0.35}As_{0.73}P_{0.27}$ quarter-wave layers. The absorber was grown with $In_{0.58}Ga_{0.42}As_{0.9}P_{0.1}$ and covered with a cap layer of InP. The cap layer is used to prevent carrier trapping and recombination at the semiconductor surface.[12] All absorbers were measured with a pump-probe experiment to have a recovery time >5 ns. For the top reflector we use a SiO_2/HfO_2 coating with a high reflectivity for the pump wavelength and a designed transmittance for the laser wavelength (Table 1).

D. Optimization of Top Reflector

Let us compare two SESAMs that have different transmittance T_t of the top reflector but with the same modulation depth of the final structure. That means the SESAM with the higher top-mirror reflectivity has a thicker absorber. As long as both SESAMs can still be fully saturated, the resulting laser performance will be the same. However, the lower transmittance T_t reduces the pulse fluence on the absorber and thus increases the damage threshold.

We calculate the top reflector needed to prevent the SESAM from damage. The damage fluence F_d of the absorber is assumed to be known. Measurements for 1.5-μm absorber material will be presented in Section 5. Equation (3) can be used to calculate the fluence on the absorber

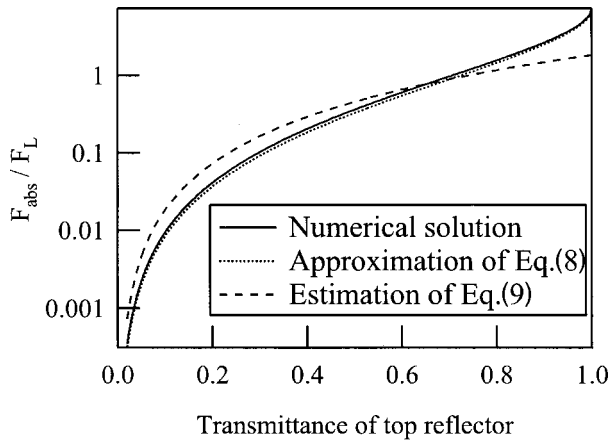

Fig. 4. Pulse fluence on the absorber divided by the saturation fluence of the gain medium plotted versus the transmittance of the top reflector. The parameters used are nonsaturable losses of $l_{ns,AR} = 20\%$, modulation depth of the AR-coated sample $\Delta R_{AR} = 40\%$, transmittance of the output coupler $T_{OC} = 10\%$, and intracavity losses of $l_{par} = 1\%$. The solid curve is a numerical simulation, the dotted curve represents Eq. (8) (neglecting the nonsaturable losses for the scaling of the modulation depth), and the dashed curve is the solution for a rough estimate given in Eq. (9).

$$F_{abs} = \frac{\xi_{high}}{T_{OC}} F_p, \tag{7}$$

where $F_p = E_p/A_L$ is the pulse fluence outside the cavity. The transmittance of the output coupler T_{OC} accounts for the fact that the SESAM is exposed to the intracavity intensity.

Using the pulse fluence described in Eq. (1) and replacing the modulation depth with the approximation of (6), we obtain a fluence on the absorber layer of

$$F_{abs} = 2F_L \Delta R_{AR} \frac{1}{(T_{OC} + l_{par})} \frac{T_t^2}{\{1 + [(1 - T_t)R_{ns,AR}]^{1/2}\}^2 \{1 + [(1 - T_t)(R_{ns,AR} - \Delta R_{AR})]^{1/2}\}^2}. \tag{8}$$

Table 1. SESAM Parameters[a]

SESAM No.	d_{abs} nm	T_t %	ΔR_{AR} %	$l_{ns,AR}$ %	ΔR %
1	40	8	5.7	1.2	0.12
2	40	12	5.7	1.2	0.19
3	40	29	5.7	1.2	0.50
4	90	8	7.4	5.4	0.17
5	90	12	7.4	5.4	0.25
6	310	8	15	16	0.37
7	310	12	15	16	0.57
8	740	8	29	27	0.87
9	740	12	29	27	1.32
Optimized	2500	5	35	60	1.17

[a] d_{abs} is the absorber thickness, and T_t is the transmittance of the top reflector. ΔR_{AR} is the modulation depth and $l_{ns,AR} = 1 - R_{ns,AR}$ are the nonsaturable losses of the AR-coated reference sample, respectively. ΔR is the modulation depth of the SESAM.

To avoid damage we should keep the fluence on the absorber below the damage fluence: $F_{abs} < F_d$.

For a rough estimate one can neglect the parasitic losses l_{par} (which should be small compared with the transmittance of the output coupler) and replace the parentheses in the second denominator with an intermediate value of 2. We obtain a condition for the transmittance of the top reflector to prevent the SESAM from damage:

$$T_t < \left(2 \frac{F_d T_{OC}}{F_L \Delta R_{AR}}\right)^{1/2}. \tag{9}$$

In Fig. 4 the quality of the approximation made in Eq. (6) and the estimate of Eq. (9) are compared with a numerical simulation. The fluence on the absorber F_{abs} divided by the saturation fluence F_L is plotted versus the transmittance of the top reflector. The parameters used for the plot are nonsaturable losses of $l_{ns,AR} = 20\%$, modulation

depth of the AR coated sample of $R_{AR} = 40\%$, transmittance of the output coupler of $T_{OC} = 10\%$, and parasitic losses of $l_{par} = 1\%$.

The strategy to achieve high modulation depth and avoid damage for a Q-switched microchip laser can be summarized as follows: First, we grow the semiconductor part of the SESAM with as much modulation depth as we can get. This can be limited by the critical thickness for strained layers, or, for lattice matched growth, the nonsaturable losses will eventually reduce the modulation depth with a further increase of the absorber thickness. The appropriate transmittance for the top reflector can be determined with Eq. (8).

5. DAMAGE MEASUREMENTS

With this experiment we determined the damage fluence of several absorbers operated in the Q-switched laser, and we showed that damage is caused mainly by excessive pulse fluence on the absorber layer, not in the dielectric top mirror. We concluded this from a large set of damage data taken with different SESAM and laser parameters. We combined the SESAMs listed in Table 1 with output couplers with transmittances of 0.43%, 6.0%, and 11.3%. The gain medium was varied with the above mentioned glasses of 0.2–1 mm thicknesses. For the pump spot we used two settings, either with diameters of $\approx 100\,\mu$m $\times$ 105 μm or of $\approx 180\,\mu$m $\times$ 160 μm. For each set data were taken at pump powers near threshold, at an intermediate value, and at full pump power ($\approx$1 W limited by glass damage).

Out of 167 combinations investigated, 29 could not reach threshold or immediate damage to the SESAM was observed. For the rest we found stable Q-switched operation. However, in this group, we could distinguish two classes: completely damage-free setups and lasers in which we found a dependence on the transverse position. (Probably damage occurs faster at spots where some defects are already present in the absorber layer.) Thirty-five combinations are in this marginal class. Note that in the marginal cases, progressing damage can considerably increase the losses without completely destroying it. This results in a slow drop of the output power (seconds to minutes) and reduced pulse energy, while the pulse duration is unchanged. It leads to a tendency in which the pulse fluence is measured too low for these marginal cases because the intracavity losses have already increased during data acquisition.

From the measured pulse energy, the laser spot size, and reflectivities of the output coupler and top reflector of the SESAM, we calculated the fluence on the absorber layer. Figure 5(a) shows this fluence versus average power. The solid circles indicate lasers without any sign of damage, while the open circles are the marginal cases. As a visual guide, we plotted an approximate upper ($F_d = 100\,$mJ/cm^2) and a lower boundary ($F_d = 10\,$mJ/cm^2) for the damage fluence. We see that the occurrence of damage does not depend on the average output power. Apparently the peak fluence of a single pulse, which is nearly independent of the average output power, is the critical quantity, and not the pulse repetition rate. In Fig. 5(b) the pulse fluence is plotted versus the pulse width, indicating that damage occurs independent of pulse width. Figure 5(c) shows the fluence for the different SESAM samples. (The SESAM numbers correspond to Table 1.) It is surprising that even different SESAMs based on the same absorber structures (i.e., with only the top mirror varied) show damage at different fluence values. We believe that this is due to errors in the calculation of the pulse fluence on the absorber. Thickness

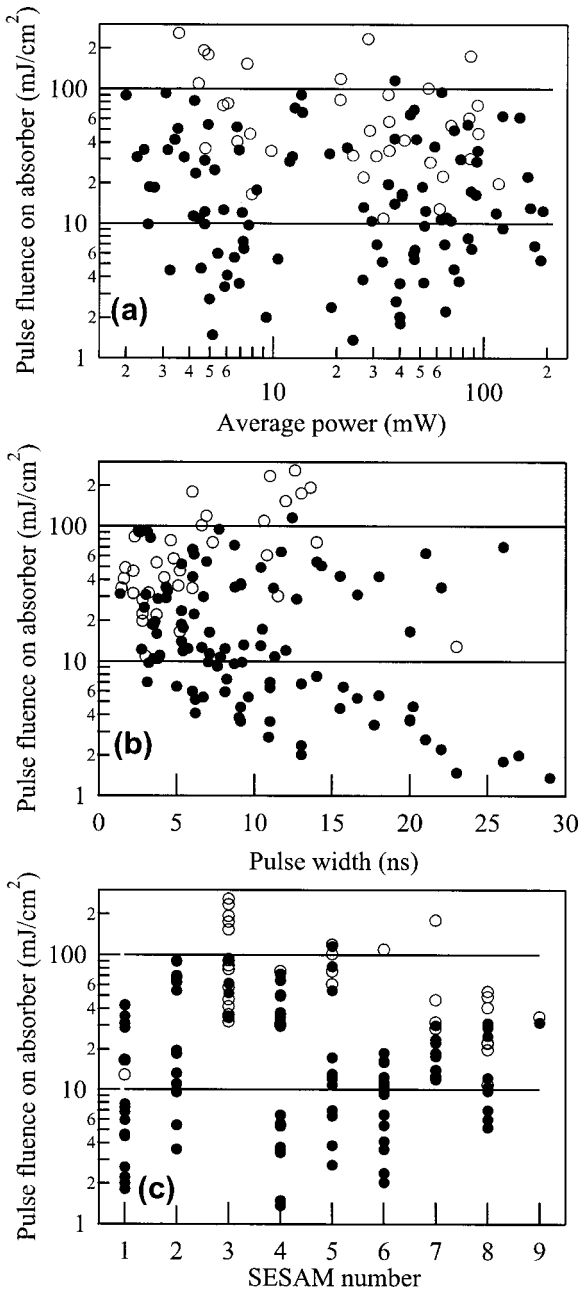

Fig. 5. Results of damage measurements under operating conditions. Each point corresponds to a result from a specific laser. In all graphs the pulse fluence on the absorber, calculated assuming antiresonance of the SESAM, belongs to the vertical axis. The solid circles indicate experiments where no damage was observed; open circles represent experiments where damage was observed only for certain spots on the absorber. The solid lines are a visual guide and indicate an upper and a lower limit for the safe parameter range. (a) Pulse fluence versus average power. (b) Pulse fluence versus pulse duration. (c) Pulse fluence versus SESAM number.

variations particularly of the thicker absorbers lead to deviations from the antiresonance condition, so that the actual fluence on the absorber can be higher than calculated assuming antiresonance.

To verify that damage occurs in the semiconductor material and not in the top reflector, we used a surface profiler (alpha-step) to investigate the damaged spots. Two kinds of profiles could be distinguished: craterlike and hill-like features. However, when the coating is removed by selective etching, the absorber below shows a similar structure for both profiles, with a hole indicating that the initial damage occurs in the absorbing layer. Note that laser-induced damage in transparent dielectric materials has been investigated extensively elsewhere,[30] but damage of semiconductor absorbers is a quite different phenomenon physically.

With this experiment we could show that damage typically occurs at a pulse fluence on the absorber above ≈10–100 mJ/cm^2.

6. OPTIMIZED SESAM AND LASER PERFORMANCE

Following the strategy discussed in Subsection 4.D for optimizing the SESAM performance leads us to the following design: On a Bragg mirror with 40 pairs of InP/InGaAsP quarter-wave layers an absorber was grown with a 2.5-μm thickness resulting in a double-pass absorption of ≈95%. For the top reflector we used $T_t = 5\%$, resulting in a modulation depth of 1.2%. An even thicker absorber of 4.5 μm was investigated with the same top reflector. However, the sample shows large nonsaturable losses, while the modulation depth could not be increased further.

The laser was set up with a 4% output coupler and a 0.5-mm thick glass doped with 2.75 wt. % Er_2O_3 and 21 wt. % Yb_2O_3. The pump spot was 170 μm × 190 μm. In Fig. 6, a sampling scope trace of the pulse is shown. The pulse has a full width at half-maximum duration of 0.84 ns, a peak power of 10.6 kW, and a pulse energy of 11.2 μJ. Figure 7 shows the optical spectrum of this pulse. With a pump power of 608 mW resulting in an output of 16 mW and a repetition rate of 1.4 kHz, nearly single-mode operation is achieved with a side-mode suppression of 15 dB. Up to 51 mW average power could be obtained (limited by glass fracture). However, above 16 mW of average power the laser could no longer be operated with a single longitudinal mode.

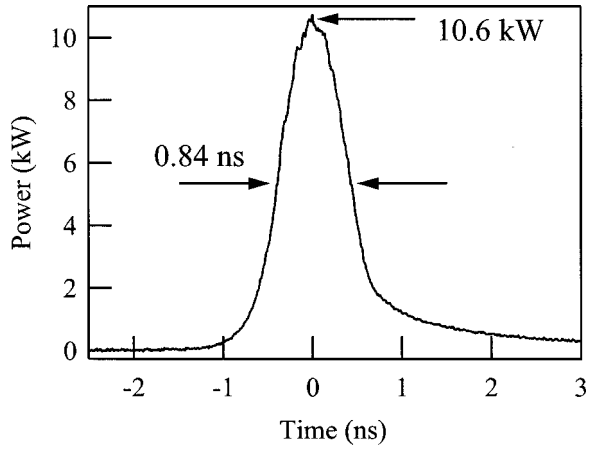

Fig. 6. Sampling scope trace of the Q-switched output pulse measured with a 45-GHz photodetector and a 50-GHz sampling head. The repetition rate was 1.4 kHz and the pulse energy 11.2 μJ resulting in an average power of 16 mW.

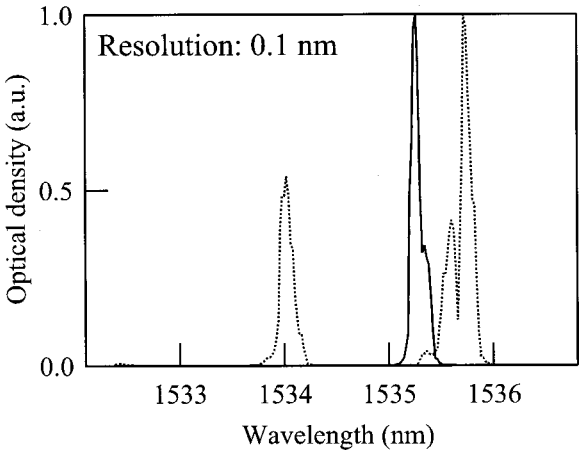

Fig. 7. Optical spectrum of the laser corresponding to the pulses shown in Fig. 6. The solid line shows a single longitudinal mode for 16-mW average power, while multi-longitudinal-mode operation is observed at higher powers (dotted curve, 45 mW). The shoulders of the peaks (particularly the single-mode peak) indicate the presence of some higher-order transverse modes.

For all setups we observed a dependence of the pulse-to-pulse jitter on the mode number. When the laser operates on a single longitudinal mode, the repetition rate typically has fluctuations below 2% (standard deviation). For operation on two longitudinal modes, the timing fluctuations become much stronger, typically around 10%, but sometimes even 30% and more. Here we often observe a hopping between two different pulse separations, either regularly or sometimes in a chaotic manner. This can be explained by spatial hole burning: When the laser reaches threshold, the longitudinal mode closest to the gain peak starts oscillating. After evolution of this first pulse, the remaining inversion is spatially modulated. Another longitudinal mode may reach threshold earlier, when it has a better overlap with the undepleted inversion. With several modes (>5) the jitter is weaker than with only two modes, but the variations typically remain much larger than in the single-mode case.

We measured a laser spot diameter of 150 μm × 115 μm in the laser. With this large mode the laser was no longer diffraction limited. We measured M^2 values of 2.0 and 2.7 parallel to the fast and slow axis of the pump diode, respectively. With pump spots of ~100 μm diameter we got close to the diffraction limit with $M^2 < 1.3$. For the 11.2-μJ pulses the fluence on the absorber was 130 mJ/cm^2. That was in the marginal regime, and indeed we also found spots where the SESAM was damaged. However, once the laser was running, we did not see any sign of degradation during the experiment, which lasted for several hours. Since there is no polarization-dependent element in the cavity, one would expect an unpolarized beam. However, with some ellipticity of the pump beam, e.g., with the pump spot diameter in one direction being 30% smaller than in the other

direction, enough strain is generated to stabilize a linear polarization state. For nearly circular pump beams, hopping between two linear polarization states can occur.

7. CONCLUSIONS

We have shown that the damage of InP/InGaAsP semiconductor saturable absorber mirrors (SESAMs) used for eye-safe passively Q-switched microchip lasers at 1.5 μm is basically determined by a critical fluence of the order of 10–100 mJ/cm^2 for a single pulse within the absorber layer. We can obtain significantly higher pulse energies of up to 11.2 μJ from such microchip lasers by using antiresonant SESAM designs with relatively high top-mirror reflectivity and a thick absorber layer, so that the fluence within the absorber layer is much smaller than the fluence incident on the SESAM. Pulses with subnanosecond duration and peak powers up to 10.6 kW have been obtained and make these lasers interesting for applications such as range finding and three-dimensional imaging.

ACKNOWLEDGMENTS

We thank Nortel Networks in Zürich, Switzerland, for providing the pump diode for these experiments. This work was supported by the Swiss Priority Program in Optics (SPO II).

The e-mail address for R. Häring is haring @iqe.phys.ethz.ch.

*R. Fluck is now with Lawrence Livermore National Laboratory, P.O. Box 808, L-438, Livermore, California 94550, USA.

REFERENCES

1. J. J. Zayhowski and A. L. Wilson, "Miniature sources of subnanosecond 1.4–4.3 μm pulses with high peak power," in *Advanced Solid-State Lasers*, H. Injeyan, U. Keller, and C. Marshall, eds., Vol. 34 of OSA Trends in Optics and Photonics Series (Optical Society of America, Washington, D.C., 2000), pp. 308–311.
2. J. J. Zayhowski, "Periodically poled lithium niobate optical parametric amplifiers pumped by high-power passively Q-switched microchip lasers," Opt. Lett. **22**, 169–171 (1997).
3. J. J. Zayhowski, S. C. Buchter, and A. L. Wilson, "Miniature Gain Switched Lasers," in *Advanced Solid State Lasers*, eds., Vol. 53 of OSA Trends in Optics and Photonics Series (Optical Society of America, Washington, D.C., 2001), pp. 308–310.
4. K. V. Yumashev, I. A. Denisov, N. N. Posnov, V. P. Mikhailov, R. Moncorgé, D. Vivien, B. Ferrand, and Y. Guyot, "Nonlinear spectroscopy and passive Q-switching operation of a Co^{2+}:$LaMgAl_{11}O_{19}$," J. Opt. Soc. Am. B **16**, 2189–2194 (1999).
5. P. Thony, B. Ferrand, and E. Molva, "1.55 μm passive Q-switched microchip laser," in *Advanced Solid State Lasers*, W. R. Bosenberg and M. M. Fejer, eds., Vol. 19 of OSA Trends in Optics and Photonics Series (Optical Society of America, Washington, D.C., 1998), pp. 150–153.
6. K. Spariosu, R. D. Stultz, M. Birnbaum, T. H. Allik, and J. A. Hutchinson, "Er:$Ca_5(PO_4)_3F$ saturable absorber Q switch for the Er:glass laser at 1.53 μm," Appl. Phys. Lett. **62**, 2763–2765 (1993).
7. R. D. Stultz, M. B. Camargo, and M. Birnbaum, "Passive Q-switch at 1.53 μm using divalent uranium ions in calcium fluoride," J. Appl. Phys. **78**, 2959–2961 (1995).
8. R. D. Stultz, M. B. Camargo, M. Lawler, D. Rockafellow, and M. Birnbaum, "Diode-Pumped Er:Yb:glass minitransmitter," in *Advanced Solid State Lasers*, W. R. Bosenberg and M. M. Fejer, eds., Vol. 19 of OSA Trends in Optics and Photonics Series (Optical Society of America, Washington, D.C., 1998), pp. 155–158.
9. R. D. Stultz, M. B. Camargo, S. T. Montgomery, M. Birnbaum, and K. Spariosu, "U:SrF efficient saturable absorber Q switch for the 1.54 μm erbium:glass laser," Appl. Phys. Lett. **64**, 948–950 (1994).
10. M. Birnbaum, M. B. Camargo, S. Lee, F. Unlu, and R. D. Stultz, "Co:ZnSe saturable absorber Q switch for the 1.54 μm Er/Yb:glass laser," *Advanced Solid State Lasers*, C. R. Pollock and W. R. Bosenberg, eds., Vol. 10 of OSA Trends in Optics and Photonics Series (Optical Society of America, Washington, D.C., 1997), pp. 148–151.
11. A. V. Podlipensky, V. G. Shcherbitsky, N. V. Kuleshov, V. P. Mikhailov, V. I. Levchenko, and V. N. Yakimovich, "Cr^{2+}:ZnSe and Co^{2+}:ZnSe saturable-absorber Q switches for 1.54-μm Er:glass," Opt. Lett. **24**, 960–963 (1999).
12. R. Fluck, R. Häring, R. Paschotta, E. Gini, H. Melchior, and U. Keller, "Eyesafe pulsed microchip laser using semiconductor saturable absorber mirrors," Appl. Phys. Lett. **72**, 3273–3275 (1998).
13. S. Kück, K. Petermann, U. Pohlmann, and G. Huber, "Near-infrared emission of Cr^{4+}-doped garnets: Lifetimes, quantum efficiencies, and emission cross sections," Phys. Rev. B **51**, 17323–17331 (1995).
14. A. Diening, P. E.-A. Möbert, and G. Huber, "Diode-pumped continuous-wave, quasi-continuous wave, and Q-switched laser operation of Yb^{3+}, Tm^{3+}:$YLiF_4$ at 1.5 and 2.3 μm," J. Appl. Phys. **84**, 5900–5904 (1998).
15. R. Brinkmann, W. Sohler, and H. Suche, "Continuous-wave erbium-diffused $LiNbO_3$ waveguide laser," Electron. Lett. **27**, 415–416 (1991).
16. S. Taccheo, P. Laporta, S. Longhi, O. Svelto, and C. Svelto, "Diode-pumped bulk erbium-ytterbium lasers," Appl. Phys. B **63**, 425–436 (1996).
17. U. Keller, D. A. B. Miller, G. D. Boyd, T. H. Chiu, J. F. Fergusson, and M. T. Asom, "Solid-state low-loss intracavity saturable absorber for Nd:YLF lasers: an antiresonant semiconductor Fabry–Perot saturable absorber," Opt. Lett. **17**, 505–507 (1992).
18. U. Keller, K. J. Weingarten, F. X. Kärtner, D. Kopf, B. Braun, I. D. Jung, R. Fluck, C. Hönninger, N. Matuschek, J. Aus der Au, "Semiconductor saturable absorber mirrors (SESAMs) for femtosecond to nanosecond pulse generation in solid-state lasers," IEEE J. Sel. Top. Quantum Electron. **2**, 435–453 (1996).
19. U. Keller, in *Nonlinear Optics in Semiconductors II: Semiconductors and Semimetals*, E. Garmire and A. Kost, eds. (Academic, Boston, 1999), **59**, pp. 211–286.
20. G. J. Spühler, R. Paschotta, R. Fluck, B. Braun, M. Moser, G. Zhang, E. Gini, and U. Keller, "Experimentally confirmed design guidelines for passively Q-switched microchip lasers using semiconductor saturable absorbers," J. Opt. Soc. Am. B **16**, 376–388 (1999).
21. B. Braun, F. X. Kärtner, M. Moser, G. Zhang, U. Keller, "56-ps passively Q-switched diode-pumped microchip laser," Opt. Lett. **22**, 381–383 (1997).
22. B. Braun, F. X. Kärtner, U. Keller, J.-P. Meyn, and G. Huber, "Passively Q-switched 180 ps Nd:LSB microchip laser," Opt. Lett. **21**, 405–407 (1996).
23. R. Fluck, B. Braun, E. Gini, H. Melchior, and U. Keller, "Passively Q-switched 1.34 μm Nd:YVO_4 microchip laser using semiconductor saturable-absorber mirrors," Opt. Lett. **22**, 991–993 (1997).
24. J. J. Zayhowski and A. Mooradian, "Single-frequency microchip Nd lasers," Opt. Lett. **14**, 24–26 (1989).
25. F. Salin and J. Squier, "Gain guiding in solid-state lasers," Opt. Lett. **17**, 1352–1354 (1992).

26. J. J. Zayhowski, "Thermal guiding in microchip lasers," in *Advanced Solid-State Lasers*, H. P. Jenssen and G. Dube, eds., Vol. 6 of OSA Proceedings Series (Optical Society of America, Washington, D.C., 1990), pp. 9–13.
27. R. Häring, R. Paschotta, E. Gini, H. Melchior, and U. Keller, "Sub-nanosecond pulses from passively *Q*-switched microchip lasers at 1.53 μm," in *Conference on Lasers and Electro-Optics* (CLEO/VS) 1999 OSA Technical Digest Series (Optical Society of America, Washington, D.C., 1999), pp. 518–519.
28. J. J. Zayhowski, P. L. Kelley, "Optimization of *Q*-switched Lasers," IEEE J. Quantum Electron. **27**, 2220–2225 (1991).
29. L. R. Brovelli, U. Keller, T. H. Chiu, "Design and operation of antiresonant Fabry–Perot saturable semiconductor absorbers for mode-locked solid-state lasers," J. Opt. Soc. Am. B **12**, 311–322 (1995).
30. B. C. Stuart, M. D. Feit, S. Herman, A. M. Rubenchik, B. W. Shore, M. D. Perry, "Nanosecond-to-femtosecond laser-induced breakdown in dielectrics," Phys. Rev. B **53**, 1749–1761 (1996).